Optimization of image quality and accuracy of low iodine concentration quantification as function of kVp pairs for abdominal imaging using dual-source CT: A phantom study

Djamel Dabli, Julien Frandon, Aymeric Hamard, Asmaa Belaouni, Takieddine Addala, Jean-Paul Beregi, Joël Greffier

Version of Record: https://www.sciencedirect.com/science/article/pii/S1120179721002520
Manuscript_f26f09876f0bf8eb1e9bcde90403de8c

Optimization of image quality and accuracy of low iodine concentration quantification as function of kVp pairs for abdominal imaging using dual-source CT: a phantom study.

D. Dabli[1 *], J.Frandon[1], A. Hamard[1], A. Belaouni[1], T. Addala[1] , J.P. Beregi[1], J. Greffier[1,]

1. Department of medical imaging, CHU Nimes, Univ Montpellier, Medical Imaging Group Nimes, EA 2992, France

* Corresponding author : Djamel DABLI, CHU de Nîmes, Medical Imaging Group Nîmes, EA 2992, Bd Prof Robert Debré, 30029 Nîmes Cedex 9; tel: +33.785.729.946; fax: +33.466.683.308; mail: djamel.dabli@chu-nimes.fr

Optimization of image quality and accuracy of low iodine concentration quantification as function of kVp pairs for abdominal imaging using dual-source CT: a phantom study.

Abstract

Purpose:

To determine the suitable kVp pair for optimal image quality of the virtual monochromatic images (VMIs) and iodine quantification accuracy at low concentration, using a third generation dual-source CT (DSCT).

Materials and methods:

Multi-energy CT phantoms with and without body rings were scanned with a DSCT using four kVp pairs (tube "A"/"B" voltage): 100/Sn150, 90/Sn150, 80/Sn150 and 70/Sn150 kVp. The reference mAs was adjusted to obtain a $CTDI_{vol}$ close to 11mGy. HU values accuracy ($RMSD_{HU}$), noise (SD) and contrast-to-noise ratio (CNR) of iodine inserts of 0.5, 1, 2 and 5mg/mL concentrations were assessed on VMIs at 40/50/60/70 keV. Iodine quantification accuracy was assessed using the $RMSD_{iodine}$ and iodine bias (IB_{iodine}).

Results:

The $RMSD_{HU}$ decreased when the tube "A" voltage increased. The mean noise value increased significantly with tube "A" voltage ($p<0.001$) but decreased between 80/Sn150 and 90/Sn150 kVp for the small phantom (1.1±0.1%; $p=0.047$). The CNR significantly decreased with tube "A" voltage ($p<0.001$), except between 80/Sn150 and 90/Sn150 kVp for all inserts and between 90/Sn150 kVp and 100/Sn150 kVp for the 1.0 and 0.5mg/mL inserts in the

large phantom. In the small phantom, no significant difference was found between 80/Sn150 kVp and 90/Sn150 kVp for all inserts and between 80/Sn150, 90/Sn150 and 100/Sn150 kVp for the 1 and 0.5mg/mL inserts. The $RMSD_{iodine}$ and IB_{iodine} decreased as the tube "A" voltage of the kVp pair increased.

Conclusion:

The kVp pair of 70/Sn150 led to better image quality in VMIs and sufficient iodine accuracy.

Keywords:

Dual-Source CT scan; Iodine quantification; Virtual monochromatic images, Contrast-to-noise ratio.

Abbreviations

CT: Computed Tomography

$CTDI_{vol}$: Volume CT dose index

DECT: Dual-energy CT

DSCT: Dual-source CT

HU: Hounsfield Unit

IB: Iodine bias

RMSD: Root-mean square deviation

VMI: Virtual monochromatic images

CNR: Contrast-to-noise ratio

SD: Standard deviation.

Introduction

The clinical interest of dual-energy in abdominal imaging and other anatomic regions is now acquired and demonstrated by several studies [1-9]. Indeed, this technique uses two spectra of X-rays, of low energy and high energy, to differentiate the attenuation of two different materials. It also allows performing a spectral analysis and quantifying the iodine concentration on specific iodine images.

Several techniques of dual-energy CT (DECT) have been developed by the manufacturers with variable spectral performances [10-13]. In the Dual-source CT (DSCT) scans, two X-ray tubes associated with two detectors are used. Each of the X-ray tubes delivers a spectrum of X-rays with the low voltage (kVp) tube (tube "A") and high voltage tube (tube "B"). Virtual monochromatic images (VMIs) are calculated as a linear combination of the basis material images using attenuation coefficients that approximate the energy dependence of the photoelectric and the Compton effects. These images improve the lesion contrast using low energy level values (from 40 to 70 keV) and reduce image artefacts with high energy level values. Also, material specific images are generated such as iodine images to quantify iodine concentration. These additional images are useful for clinical applications in abdominal imaging to detect and characterize the lesions [14-18].

Five kVp pairs are now available in the third generation DSCT, among them four pairs use a tin filter with the high-energy spectrum delivered by tube "B". This compensates the limit related to the tube power at low-kVp [19] during acquisitions on large patients and improves the spectral separation [20] by increasing the gap between the low and high-energy spectra.

The default kVp pair set by the manufacturer in DSCT for abdominal imaging is the 100/Sn150 kVp pair, which may be changed by the users depending of the patient morphology for example. However, changing the kVp pair could affect the spectral quantities and image quality. Few studies have assessed this impact [21-22]. Krauss *et al.* [19] assessed the impact of the kVp pairs on the spectral separation of iodine material and the noise level of the mixed and virtual non-contrast images using different phantom sizes. Another study by Pelgrim et al. [22] assessed the accuracy of iodine quantification as

function of the kVp pairs in the third generation DSCT using semi-anthropomorphic phantom simulating a human thorax. However, these studies used iodine concentrations higher than 2 mg/mL. Nevertheless, the concentration measured in clinical applications for abdominal lesions are in general lower than 5 mg/mL [14-18] and the reported diagnostic threshold to differentiate lesions ranged between 0.9 mg/mL [14, 15] to 2 mg/mL [16]. Then, assessing the accuracy of quantification of low iodine concentrations (< 2mg/mL) as function of kVp pairs is still required.

The purpose of this study was to assess the impact of four kVp pairs (using tin filter) in a third generation DSCT on the HU accuracy, image quality in VMIs and iodine quantification at low iodine concentrations.

Materials and methods

Phantoms

A Multi-Energy CT phantom (Sun Nuclear, Middleton, WI) composed of 16 removable inserts (diameter of 2.85 cm) placed into a water equivalent background material was used. This phantom of 20 cm diameter with an elliptical ring (30 cm x 40 cm x 15 cm) (**Figure1.a** and **1.b)** was used to simulate the morphology of patients undergoing an abdomen-pelvic CT examination. Both morphologies (small and large phantoms) were used to assess the accuracy of the HU values and iodine concentration. Inserts of different iodine concentration were placed in the 20-cm phantom area in the same positions for each acquisition. Ten inserts were placed in the small phantom and 16 in the large phantom (6 more inserts placed in the elliptical rings).

Acquisition and reconstruction parameters

Acquisitions were performed with a third generation DSCT (Somatom Force, Siemens Healthineers, Forcheim, Germany). The acquisition parameters of classic abdomen-pelvic examination were used: a rotation time of 0.5 s/rot, pitch factor of 0.6, and beam collimation of 128 x 0.6 mm. Four pairs of low-kVp in tube "A" and high-kVp in tube "B" with an available tin filter with thickness of 0.6 mm were used: 100/Sn 150 kVp, 90/Sn 150 kVp, 80/Sn 150 kVp and 70/Sn 150 kVp.

For each kVp pair, the tube current (mAs) was adjusted for tube "A"; as the tube "B" mAs are computed automatically by the system and cannot be modified by the user. The tube current modulation system (CareDose 4D) was activated for each acquisition to take into account the morphologies of the phantoms used (e.g. elliptical form of body phantom). The reference mAs (mAs_{ref}) was adjusted to obtain a $CTDI_{vol}$ close to 11 mGy after longitudinal modulation defined from the 2D acquisition of the phantom (topogram). The effective mAs (mAs_{eff}) was automatically adapted during the acquisition by the

angular modulation (**Table 2**). A $CTDI_{vol}$ of 11 mGy was chosen in accordance with the guide value of the French Diagnostic Reference Level for abdomen pelvic CT examination.

The raw data were reconstructed with level 3 ADMIRE (A3) using the standard soft tissue reconstruction kernel (Br40) usually used for abdomen-pelvic exploration. Images were reconstructed with slice thickness close to 1 mm (1-mm increment) and a field of view of 420 mm for both phantoms. These reconstruction parameters are used in clinical practice for abdomen-pelvis CT examination and were used in this study in the reconstruction process of all types of images assessed.

For each kVp pair, the phantoms were scanned three times with the same acquisition and reconstruction parameters. Virtual monochromatic images (VMI) at 40, 50, 60 and 70 keV were generated using the "Monoenergetic +" application on the Syngo-Via workstation. These three energy levels were chosen because they are routinely used for improving the iodine contrast. Iodine concentration images were also computed using the "Virtual Unenhanced" application.

Virtual monochromatic attenuation

HU accuracy and noise assessment

For each of the three CT acquisitions performed, the HU values were measured in a single slice positioned in the center of the Multi-Energy CT phantom by semi-automatically placing one circular region of interest (ROI; 2-cm diameter) on the solid water insert and on four iodine inserts with an iodine concentration of 0.5, 1.0, 2.0 and 5.0 mg/mL (**Figure 2.a and 2.b**). For each insert, the HU value (mean attenuation of pixels within each ROI) and noise

value (SD, corresponding to the standard deviation of mean HU within each ROI) were computed for monochromatic images at 40, 50, 60 and 70 keV. The elemental composition of each insert is depicted in the **supplementary material**.

The accuracy of the HU values at each energy level and for each kVp pair was obtained using the root-mean-square deviation ($RMSD_{HU}$) between the measured and theoretical HU values according to the following formula:

$$RMSD_{HU} = \sqrt{\frac{\sum_{i=1}^{K}\left(\left((HU_k)_{measured} - (HU_k)_{theoretical}\right)\right)^2}{K}} \qquad (1)$$

where, HU_k corresponds to the mean HU value of each insert (0.5, 1, 2, and 5 mg/mL) and K the number of inserts. It was calculated for each energy level and the two phantoms used.

To characterize the noise generated in iodine inserts for each kVp pair, a mean SD value was calculated and compared over the four inserts for each kVp pair and each phantom.

Contrast-to-noise ratio:

The contrast-to-noise ratio (CNR) was calculated using the following formula (2) for the iodine concentration inserts (0.5, 1, 2 and 5 mg/mL):

$$CNR = \frac{|HU_{ROI} - HU_{Ref}|}{\sqrt{\frac{\left((SD)^2_{ROI} + (SD)^2_{Ref}\right)}{2}}} \qquad (2)$$

where HU_{ROI} and $(SD)_{ROI}$ correspond to the mean HU and noise respectively measured in the ROI placed in the center of the iodine insert. HU_{Ref} and $(SD)_{Ref}$ correspond to the HU and noise values measured in a solid water insert.

Iodine concentration

For each of the three CT acquisitions performed, the iodine concentration was estimated in the iodine concentration images by placing a ROI (diameter of 2 cm) in the center of the four iodine inserts (**Figure 2.c and 2.d**).

The accuracy of the iodine concentration was obtained using the root-mean-square deviation ($RMSD_{iodine}$) between the measured and theoretical iodine concentration values using the following formula (3):

$$RMSD_{iode} = \sqrt{\frac{\sum_{i=1}^{K}(c^{i}_{theoretical} - c^{i}_{measured})^{2}}{K}}, \qquad c^{1,\dots,K} = 0.5, 1, 2 \; and \; 5 \; mg/ml. \quad (3)$$

where $c^{i}_{theoretical}$ and $c^{i}_{theoretical}$ are the theoretical and measured iodine concentration values corresponding to the *i* insert. K is the number of iodine inserts.

The iodine bias (IB) was used to characterize each kVp pair overall deviation from the nominal concentration [2] and was computed, as follows (4):

$$IB = \sum_{i=0.5,1,2,5} ([I]_i - i), \qquad (4)$$

where *i* is the nominal iodine concentration and $[I]_i$ is the iodine concentration estimated for a given insert.

Dosimetry

Volume CT dose indexes ($CTDI_{vol}$), determined for a 32-cm diameter (polymethyl methacrylate) reference phantom, were retrieved manually from the review report available in the CT workstation at the end of the acquisitions.

Statistical analyses

Statistical analyses were performed using the R software version 3.5.1 (R Core Team (2017)). A Shapiro-Wilk test was used to verify the normality of each data distribution ($RMSD_{HU}$, CNR, mean SD). The F-test was used to test the equality of variances between data distributions obtained with different kVp pairs.

For CNR and noise (SD), all data distributions were normal (p-values vary from 0.352 to 0.940) and variance equality was confirmed between all compared distributions obtained with different kVp pairs and phantom sizes (p-value vary from 0.102 to 0.983). The paired t-Student test was then used to compare the data distribution of each quantity as function of the kVp pairs and phantom sizes.

For $RMSD_{HU}$, the distribution was not normal (p-values <0.1). Then, the Wilcoxon signed rank test for paired data was used to compare data distribution obtained with different kVp pairs and different phantom sizes.

For all statistical tests, a p-value ≤ 0.05 was considered significant.

Results

Monochromatic images

Accuracy of HU values

The measured HU values for the four energy levels for the two phantoms and the theoretical values are depicted in **Table 1**. The $RMSD_{HU}$ values for both phantoms as function of kVp pairs and low energy levels are depicted in **Figure 3**. For both phantoms, the $RMSD_{HU}$ decreased when the energy level increased for all kVp pairs. The lowest values of $RMSD_{HU}$ were found for 100/Sn150 kVp for the two phantoms.

For both phantoms, the $RMSD_{HU}$ decreased when the tube "A" voltage increased. For all keV and for the two phantoms, the mean $RMSD_{HU}$ values decreased significantly between kVp pairs (p<0.001) , except between 80/Sn150 kVp and 90/Sn150 kVp pairs (mean difference: 2.8 ± 0.1%; p=0.909) for the large phantom.

For all kVp pairs and energy levels, the $RMSD_{HU}$ values were significantly higher for the large phantom than for the small phantom (p<0.001).

Image noise

The mean noise values among all iodine inserts as function of the kVp pairs and low energy levels are presented in **Figure 4**.

For both phantoms, the mean noise values decreased when the energy level increased for all kVp pairs.

For both phantoms, the mean noise values increased significantly when the tube "A" voltage increased for all kVp pairs (p<0.001) but decreased significantly between 80/Sn150 kVp and 90/Sn150 kVp for the small phantom (mean difference: 1.1 ± 0.1%; p=0.047). It decreased but not significantly between 90/Sn150 kVp and 100/Sn150 kVp for the large phantom (mean difference: 1.8 ± 0.1%).

For all kVp pairs and energy levels, the mean noise values were significantly higher for the large phantom than for the small phantom (p<0.001).

Contrast-to-noise ratio:

The CNR values measured in both phantoms for the four-iodine concentration inserts are depicted in the **Figure 5**.

For both phantoms and all kVp pairs, the CNR values decreased when the energy level increased and the iodine concentration decreased.

For the large phantom and all iodine inserts, CNR values were significantly decreased as the tube "A" voltage of the kVp pair increased (p<0.001), except between 80/Sn 150 kVp and 90/Sn 150 kVp for all inserts and between 90/Sn150 kVp and 100/Sn150 kVp for the 2.0; 1.0 and 0.5 mg/mL inserts. For the small phantom, CNR values were significantly decreased as the tube "A" voltage of the kVp pair increased (p<0.001), except between 80/Sn 150 kVp and 90/Sn 150 kVp for all inserts and between 80/Sn 150, 90/Sn 150 and 100/Sn 150 kVp for the 1 and 0.5 mg/mL inserts, where CNR values were in the same range.

The CNR values were significantly higher in the small phantom compared to the large one for all energy levels and kVp pairs (p<0.001). The decrease of CNR values between the small and large phantoms was of -64.8% ± 3.0%, similar for all kVp pairs, energy level and iodine inserts.

Iodine images

The measured iodine concentrations were higher than their respective theoretical values for both phantoms, for all kVp pairs and all iodine concentrations (**Table 2**). The $RMSD_{iodine}$ and IB decreased as the tube "A" voltage of the kVp pair increased. The $RMSD_{iodine}$ values were lower for the small phantom than for the large phantom for all kVp pairs (-4% for 80/Sn 150 kVp and -29% for 100/Sn 150 kVp) The IB values were in the same range for both phantoms for all kVp pairs, except for 100/Sn 150 kVp where IB was lower for the small phantom.

Dosimetry

CTDIvol and the effective mAs obtained with different kVp pairs in both phantoms are depicted in Table 1.

For all dose levels, the effective "mAs" of tube "A" were higher than of tube "B". The effective "mAs" of the two tubes decreased in the same proportion when the CTDIvol decreased. The mAs ratio between tube"A" and tube "B" was the same for all dose levels.

Discussion

This study demonstrated that the increase of tube "A" voltage of the kVp pair increased the image noise, reduced the CNR and improved the accuracy of HU values and iodine quantification. For all metrics assessed, better outcomes were found with the small phantom than with the large one.

The decrease of the $RMSD_{HU}$ values was related to the overestimation of the measured HU values compared with their respective theoretical values when the tube "A" voltage decreased. These variations were stronger with high iodine concentrations (2 and 5 mg/mL) and affected the $RMSD_{HU,}$ as it takes into account the HU value of all iodine inserts. This behavior could be explained by the high contribution of the low kVp spectrum in the calculation of HU values at low energy levels in VMIs. Indeed, VMIs are calculated as a linear combination of the basis material images using attenuation coefficients that approximate the energy dependence of the photoelectric and the Compton effects. Then, when the tube "A" voltage decreased, the contribution of the photoelectric effect at low energy level increased and could lead to an overestimation of the calculated HU value, particularly at high-density material.

The increase of the noise with the tube "A" voltage of the kVp pairs for both phantoms could be related to the spectral separation of each kVp pair. Indeed, the ability of DSCT to separate two materials is dependent on the spectral separation of the X-ray beam, characterized by the difference between the tube "A" and tube "B" voltages [10]. The kVp pair presenting a higher spectral separation (70/Sn 150 kVp) led to the lowest noise values. Finally, we found that the noise decreased as the energy levels increased.

The decrease in CNR along with the energy level and its decrease as the tube "A" voltage of the kVp pair increased were directly related to the outcomes of HU accuracy and noise values for each kVp pair. Indeed, lowest noise values and highest iodine HU values were found with 70/Sn150 kVp and

the opposite with 100/Sn150 kVp. Globally, the CNR variations according to the kVp pairs were higher in the large phantom than in the small phantom and depended on the iodine concentration. This outcome is due to the high beam attenuation resulting in the high noise in the large phantom..

Concerning the iodine quantification, our results suggest that the most accurate iodine measurements were obtained with the 100/Sn150 kVp pair in both phantoms. However, the $RMSD_{iodine}$ values were in the range of 0.12 to 0.34, which reflects a low error on iodine quantification for all kVp pairs even at 70/Sn 150 kVp, taking into account the concentrations encountered in clinical applications [14-18]. Jacobsen *et al.* [13] found similar overestimations of the iodine concentrations and IB for the 100/Sn150 kV pair; for the 90/Sn150 kVp pair, they found a negative IB. The differences could be related to the different iodine concentration inserts (2, 5 and 15 mg/mL) and higher dose levels than in our study. Another study compared the iodine quantification for the same kVp pairs using semi-anthropomorphic phantom equipped with 15-mL tubes manually filled with diluted contrast solutions. Pelgrim *et al.* [22] found that the most accurate iodine quantification were obtained for the protocols using the 70/Sn150 and 80/Sn150 kVp pairs. However, the conception of the phantom used and the dose level variations according to the kVp pair (from 18.7 mGy at 70/Sn150 kVp to 32.2 mGy at 100/Sn150 kVp) do not allow putting our results in regards.

Finally, our results suggest favoring the 70/Sn150 kVp pair for abdominal imaging. We showed that this kVp pair is the most suitable for the visualization of VMI at low-keV (below 70 keV) and lead to sufficiently accurate iodine quantification. Indeed, for these energy levels, iodine contrast enhancement improved the detection and quantification of the injected lesions, such as renal cell carcinomas or focal liver lesions. Our study also showed that CNR was better with the 70/Sn 150kVp pair, the one with the greatest spectral separation. However, it is important to note that the results obtained here are related to the morphology of phantom used. Indeed, we chose two phantom configurations, with or without body ring to represent both a thin and a standard patient undergoing an abdomen-pelvic CT examination. However, Michalak *et al.* have shown that the spectral performance obtained for different kVp pairs

changed as function of the width of the phantoms [21]. They reported more image noise with larger phantoms (or patients) and recommended using 90/Sn150 kVp for phantoms above 40 cm wide to improve VMIs. Our results showed that if the patient size required an increase in the tube "A" voltage, it was possible to use a 90/Sn150 kVp pair, which led to similar results in terms of CNR than the 80Sn/150 kVp pair, with accurate iodine quantification. In case of lesions with iodine concentrations lower than 2 mg/mL, the use of the 100Sn/150 kVp pair led to similar results than the 90/Sn150 kVp pair, with higher iodine quantification accuracy.

This study has several limitations. First, all acquisitions were performed on phantoms that did not take into account of the patients' movements and heterogeneities. Also, only one dose level, a single standard soft tissue reconstruction kernel and a single iterative reconstruction level were used. In addition, the metrics used did not allow the assessment of the image texture impact and the spatial resolution; we focused on the CNR and iodine quantification, which are relevant parameters to compare different acquisitions. Finally, the effect of the iodinated volume on the measured iodine concentration was not taken into account in our study. Indeed, when the size of iodinated vascular volume is small, as frequently is in abdominal iodinated vasculatures, iodine content may be significantly underestimated.

Conclusion

This study showed that the 70/Sn150 kVp pair allowed both better image quality in VMIs and acceptable iodine accuracy. However, in case an increase in the tube "A" voltage is required due to patient's size, the use of a 90 kVp may be more suitable, as it showed similar CNR and sufficient iodine quantification accuracy than at 80 kVp. For the concentrations below 2 mg/mL, the use of 100/Sn 150 kVp leads to similar results than 90/Sn 150 kVp.

Acknowledgments

We thank Dr H. de Forges for her help in preediting the manuscript.

References

[1] Moritz H. Albrecht, MD • Thomas J. Vogl, MD • Simon S. Martin, MD et al « Review of Clinical Applications for Virtual Monoenergetic Dual-Energy CT » Radiology 2019; 293:260–271 Radiology. 2014;271:327-42.

[2] Heye T, Nelson RC, Ho LM, Marin D, Boll DT. Dual-energy CT applications in the abdomen. AJR Am J Roentgenol. 2012;199:S64-70.

[3] Lestra T, Mule S, Millet I, Carsin-Vu A, Taourel P, Hoeffel C. Applications of dual energy computed tomography in abdominal imaging. Diagn Interv Imaging. 2016;97:593-603.

[4] Hanson GJ, Michalak GJ, Childs R, McCollough B, Kurup AN, Hough DM, et al. Low kV versus dual-energy virtual monoenergetic CT imaging for proven liver lesions: what are the advantages and trade-offs in conspicuity and image quality? A pilot study. Abdom Radiol (NY). 2018;43:1404-12

[5] Nicolas Murray, Kathryn E. Darras, Frances E. Walstra, Mohammed F. Mohammed, Patrick D. McLaughlin, Savvas Nicolaou. Dual-Energy CT in Evaluation of the Acute Abdomen. RadioGraphics 2019; 39:264–286.

[6] Marin D, Boll DT, Mileto A, Nelson RC. State of the art: dual-energy CT of the abdomen. Radiology. 2014 May;271(2):327-42. doi: 10.1148/radiol.14131480. PMID: 24761954.

[7] Zhang Y, Cheng J, Hua X, Yu M, Xu C, Zhang F, Xu J, Wu H. Can Spectral CT Imaging Improve the Differentiation between Malignant and Benign Solitary Pulmonary Nodules ? PLoS One. 2016 Feb 3;11(2):e0147537. doi: 10.1371/journal.pone.0147537. PMID: 26840459; PMCID: PMC4739615

[8] Marin D, Boll DT, Mileto A, Nelson RC. State of the art: dual-energy CT of the abdomen. Radiology. 2014 May;271(2):327-42. doi: 10.1148/radiol.14131480. PMID: 24761954.

[9] Muenzel D, Lo GC, Yu HS, Parakh A, Patino M, Kambadakone A, Rummeny EJ, Sahani DV. Material density iodine images in dual-energy CT: Detection and characterization of hypervascular liver lesions compared to magnetic resonance imaging. Eur J Radiol. 2017 Oct;95:300-306. doi: 10.1016/j.ejrad.2017.08.035. Epub 2017 Aug 31. PMID: 28987684.

[10] Cynthia H. McCollougha, Kirsten Boedeker, Dianna Cody, Xinhui Duan, Thomas Flohr, Sandra S. Halliburton, Jiang Hsieh, Rick R. Layman, Norbert J. Pelc. Principles and applications of multienergy CT: Report of AAPM Task Group 291. Med. Phys. 47 (7), July 2020.

[11] Papadakis AE, Damilakis J. Fast kVp-switching dual energy contrast-enhanced thorax and cardiac CT: A phantom study on the accuracy of iodine concentration and effective atomic number measurement. Med Phys. 2017 Sep;44(9):4724-4735. doi: 10.1002/mp.12437. Epub 2017 Jul 25. PMID: 28658505.

[12] Greffier J, Si-Mohamed S, Dabli D, de Forges H, Hamard A, Douek P, Beregi JP, Frandon J. Performance of four dual-energy CT platforms for abdominal imaging: a task-based image quality assessment based on phantom data. Eur Radiol. 2021 Jan 15. doi: 10.1007/s00330-020-07671-2. Epub ahead of print. PMID: 33449188.

[13] Jacobsen MC, Schellingerhout D, Wood CA, Tamm EP, Godoy MC, Sun J, Cody DD. Intermanufacturer Comparison of Dual-Energy CT Iodine Quantification and Monochromatic Attenuation: A Phantom Study. Radiology. 2018 Apr;287(1):224-234. doi: 10.1148/radiol.2017170896. Epub 2017 Nov 29. PMID: 29185902.

[14] Mileto A, Marin D, Alfaro-Cordoba M, et al. Iodine quantification to distinguish clear cell from papillary renal cell carcinoma at dual-energy multidetector CT: a multireader diagnostic performance study. Radiology 2014;273(3):813–820.

[15] Zarzour JG, Milner D, Valentin R, et al. Quantitative iodine content threshold for discrimination of renal cell carcinomas using rapid kV-switching dual-energy CT. Abdom Radiol (NY) 2017;42(3):727–734.

[16] Rizzo S, Radice D, Femia M, et al. Metastatic and non-metastatic lymph nodes: quantification and different distribution of iodine uptake assessed by dual-energy CT. Eur Radiol 2018;28(2):760–769.

[17] Kato T, Uehara K, Ishigaki S, et al. Clinical significance of dual-energy CT-derived iodine quantification in the diagnosis of metastatic LN in colorectal cancer. Eur J Surg Oncol 2015;41(11):1464–1470.

[18] Pedro D. M. Lourenco, Ryan Rawski, Mohammed F. Mohammed, Faisal Khosa, Savvas Nicolaou, and Patrick McLaughlin. Dual-Energy CT Iodine Mapping and 40-keV Monoenergetic Applications in the Diagnosis of Acute Bowel Ischemia. American Journal of Roentgenology 2018 211:3, 564-570

[19] Krauss B, Grant KL, Schmidt BT, Flohr TG. The importance of spectral separation: an assessment of dual-energy spectral separation for quantitative ability and dose efficiency. Invest Radiol. 2015;50:114-8.

[20] Primak AN, Giraldo JC, Eusemann CD, Schmidt B, Kantor B, Fletcher JG, et al. Dual-source dual-energy CT with additional tin filtration: Dose and image quality evaluation in phantoms and in vivo. AJR Am J Roentgenol. 2010;195:1164-74.

[21] Michalak G, Grimes J, Fletcher J, et al. Selection of optimal tube potential settings for dual-energy CT virtual mono-energetic imaging of iodine in the abdomen [published online ahead of print 2017/04/04. Abdom Radiol (NY). 2017;42(9):2289-2296.

[22] Pelgrim GJ, van Hamersvelt RW, Willemink MJ, Schmidt BT, Flohr T, Schilham A, Milles J, Oudkerk M, Leiner T, Vliegenthart R. Accuracy of iodine quantification using dual energy CT in latest generation dual source and dual layer CT. Eur Radiol. 2017 Sep;27(9):3904-3912. doi: 10.1007/s00330-017-4752-9. Epub 2017 Feb 6. PMID: 28168368; PMCID: PMC5544802.

Table 1. Measured HU values for four energy levels in both phantoms compared to theoretical values averaged over three repeated acquisitions for iodine inserts at 5.0. 2.0. 1.0 and 0.5 mg/ml.

Phantom size			Small phantom				Large phantom			
Energy Level (keV)	**Inserts**	**Theoretical values (HU) /kVp pairs**	**70/Sn150**	**80/Sn150**	**90/Sn150**	**100/Sn150**	**70/Sn150**	**80/Sn150**	**90/Sn150**	**100/Sn150**
40.0	Iodine 5 mg/mL	426.0	455.2 ± 0.7	447.4 ± 1.4	435.9 ± 1.5	426.1 ± 0.8	464.8 ± 6.2	460.5 ± 4.8	459.8 ± 3.1	434.4 ± 4.3
	Iodine 2 mg/mL	171.0	185.7 ± 0.6	180.7 ± 0.2	173.2 ± 0.8	173.2 ± 1.5	199.5 ± 0.2	174.6 ± 1.3	178.3 ± 3.2	177.1 ± 4.7
	Iodine 1 mg/mL	88.0	100.8 ± 1.1	94.4 ± 0.3	91.2 ± 0.4	86.9 ± 0.6	88.4 ± 0.5	87.1 ± 1.0	87.8 ± 0.8	89.5 ± 2.4
	Iodine 0.5 mg/mL	46.0	53.7 ± 1.3	49.7 ± 2.0	46.5 ± 2.7	40.8 ± 1.1	46.1 ± 0.0	48.8 ± 1.7	47.2 ± 0.8	50.2 ± 4.3
50.0	Iodine 5 mg/mL	280.0	296.5 ± 0.4	291.5 ± 0.9	284.9 ± 1.1	283.9 ± 0.0	303.0 ± 4.3	299.9 ± 2.8	299.5 ± 2.5	284.5 ± 1.8
	Iodine 2 mg/mL	112.0	120.6 ± 0.4	116.7 ± 0.9	113.2 ± 0.4	113.1 ± 0.9	130.0 ± 0.3	112.8 ± 2.3	117.2 ± 1.5	116.1 ± 2.2
	Iodine 1 mg/mL	58.0	65.8 ± 0.8	61.8 ± 0.1	59.8 ± 0.4	57.4 ± 0.4	58.5 ± 0.4	56.8 ± 0.7	57.8 ± 1.8	57.4 ± 2.1
	Iodine 0.5 mg/mL	30.0	35.0 ± 0.9	32.2 ± 1.5	30.4 ± 1.6	27.2 ± 0.7	31.3 ± 0.4	32.4 ± 1.0	31.7 ± 0.3	33.0 ± 1.9
60.0	Iodine 5 mg/mL	189.0	199.9 ± 0.3	196.8 ± 0.5	193.1 ± 0.8	192.5 ± 0.4	204.6 ± 3.1	202.2 ± 1.6	202.0 ± 2.1	193.3 ± 0.5
	Iodine 2 mg/mL	75.0	81.1 ± 0.2	80.6 ± 0.4	76.7 ± 0.3	76.5 ± 0.6	87.8 ± 0.4	76.6 ± 0.6	80.1 ± 0.7	79.1 ± 1.4
	Iodine 1 mg/mL	38.0	44.5 ± 0.6	42.0 ± 0.3	40.7 ± 0.4	39.5 ± 0.3	36.5 ± 2.4	38.4 ± 0.5	38.5 ± 0.5	37.9 ± 1.8
	Iodine 0.5 mg/mL	19.0	23.6 ± 0.7	21.6 ± 1.2	20.7 ± 0.9	19.0 ± 0.5	22.3 ± 0.7	22.4 ± 0.6	22.3 ± 0.2	22.5 ± 0.5
70.0	Iodine 5 mg/mL	133.0	140.4 ± 0.2	138.3 ± 0.3	136.5 ± 0.7	134.6 ± 0.6	144.0 ± 2.4	142.0 ± 0.9	141.9 ± 1.9	137.1 ± 0.7
	Iodine 2 mg/mL	52.0	56.7 ± 0.1	56.4 ± 0.3	54.2 ± 0.4	54.0 ± 0.4	61.7 ± 0.4	56.9 ± 1.1	57.1 ± 0.8	56.2 ± 1.8
	Iodine 1 mg/mL	26.0	31.4 ± 0.5	29.7 ± 0.4	28.9 ± 0.4	28.5 ± 0.3	25.8 ± 1.7	27.1 ± 0.4	27.1 ± 0.4	25.9 ± 1.7
	Iodine 0.5 mg/mL	13.0	16.5 ± 0.6	15.0 ± 1.0	14.7 ± 0.5	13.9 ± 0.4	16.7 ± 0.9	16.2 ± 0.4	16.5 ± 0.3	16.1 ± 0.5

Values are expressed as mean ± standard deviation (SD).

Table 2. Measured iodine concentration as function of the kVp pairs for tow phantom sizes and the associated root mean square deviation ($RMSD_{iodine}$) and the iodine bias (IB) averaged over the five iodine concentrations

Phantom size	KVp pairs	Iodine concentrations				RMSDiodine	IB
		5 mg/mL	2 mg/mL	1 mg/mL	0.5 mg/mL		
Large	70/Sn150	5.60 ± 0.10	2.40 ± 0.10	1.03 ± 0.06	0.53 ± 0.06	**0.37 ± 0.01**	**1.07 ± 0.06**
	80/Sn150	5.43 ± 0.06	2.20 ± 0.00	1.07 ± 0.06	0.53 ± 0.06	**0.24 ± 0.02**	**0.73 ± 0.06**
	90/Sn150	5.47 ± 0.06	2.03 ± 0.12	1.07 ± 0.06	0.53 ± 0.06	**0.24 ± 0.03**	**0.60 ± 0.10**
	100/Sn150	5.20 ± 0.10	2.17 ± 0.06	1.03 ± 0.06	0.53 ± 0.12	**0.14 ± 0.03**	**0.43 ± 0.12**
Small	70/Sn150	5.53 ± 0.06	2.33 ± 0.06	1.20 ± 0.10	0.50 ± 0.06	**0.34 ± 0.01**	**1.07 ± 0.10**
	80/Sn150	5.40 ± 0.10	2.17 ± 0.06	1.13 ± 0.06	0.57 ± 0.06	**0.24 ± 0.02**	**0.77 ± 0.06**
	90/Sn150	5.30 ± 0.00	2.13 ± 0.06	1.10 ± 0.00	0.57 ± 0.06	**0.18 ± 0.01**	**0.60 ± 0.10**
	100/Sn150	5.20 ± 0.00	2.07 ± 0.12	1.00 ± 0.00	0.51 ± 0.06	**0.12 ± 0.03**	**0.28 ± 0.10**

Values are expressed as mean ± standard deviation (SD).

Table 3. Tube current used for tube "A" and tube "B" voltages, mAs ratio between mAs used for both tubes and volume CT dose index ($CTDI_{vol}$) used for the four pairs of kVp and for two phantom sizes.

		kVp pairs			
	Phantom size	**70/Sn150**	**80/Sn150**	**90/Sn150**	**100/Sn150**
Effective mAs	Large	567/112	309/136	215/127	182/88
	Small	444/156	250/164	187/145	169/101

mAs ratio	Large	5.1	2.3	1.7	2.1
	Small	2.8	1.5	1.3	1.7
CTDIvol	Large	10.62 ± 0.06	10.56 ± 0.01	10.60 ± 0.02	10.55 ± 0.02
	Small	10.38 ± 0.07	10.26 ± 0.03	10.29 ± 0.00	10.40 ± 0.02

$CTDI_{vol}$ values are expressed as mean ± standard deviation (SD).

Figure legends

Figure 1: a. 20 cm diameter Multi-Energy CT phantom (small phantom); **b.** Multi-Energy CT phantom with an elliptical ring 30 cm x 40 cm x 15 cm (large phantom)

Figure 2.a: Virtual monochromatic image at 70 keV of the 20 cm diameter Multi-Energy CT phantom(small phantom) with the positions of solid water and iodine inserts at 5, 2, 1 and 0.5 mg/mL; **b.** Virtual monochromatic image at 70 keV of the 20 cm diameter Multi-Energy CT phantom with an elliptical ring (large phantom); **c.**Iodine image with iodine inserts (5, 2, 1 and 0.5 mg/ml) used to determine the iodine concentration accuracy in the 20 cm diameter phantom (small phantom); **d.** Iodine image with iodine inserts (5, 2, 1 and 0.5 mg/mL) used to determine the iodine concentration accuracy in the 20 cm diameter phantom associated with the elliptical ring (large phantom).

Figure 3.a Root mean square deviation of HU values ($RMSD_{HU}$) obtained among four iodine inserts on virtual monochromatic images at 40, 50, 60 and 70 keV across the four pairs of kVp in the small phantoms size. **b.** $RMSD_{HU}$ values in the large phantom.

Figure 4.a. Mean noise values obtained among four iodine inserts on virtual monochromatic images as function of energy levels (40, 50, 60 and 70 keV) and the four pairs of kVp in the small phantom; **b**. mean noise values obtained among four iodine inserts on virtual monochromatic images as function of energy levels (40, 50, 60 and 70 keV) and the four pairs of kVp in the large phantom.

Figure 5.a. The mean CNR measured in small phantom for 5 mg/ml iodine insert. **b**. for 2 mg/ml. **c**. for 1 mg/ml. **d.** 0.5 mg/ml; **e.** The mean CNR measured in large phantom for 5 mg/ml iodine insert; **f.** for 2 mg/ml; **g.** for 1 mg/ml; **h.** for 0.5 mg/ml.

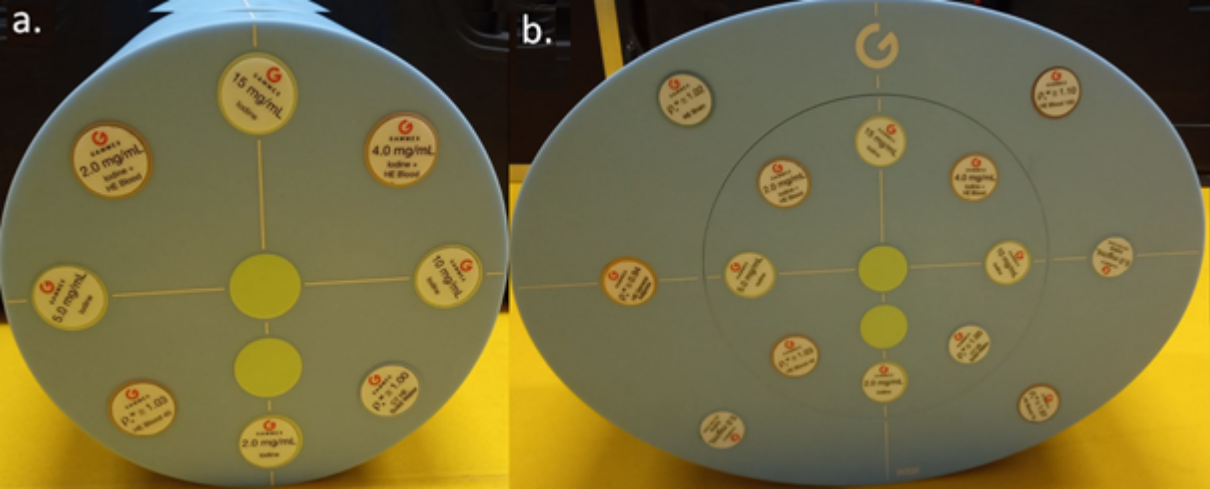
a.
b.

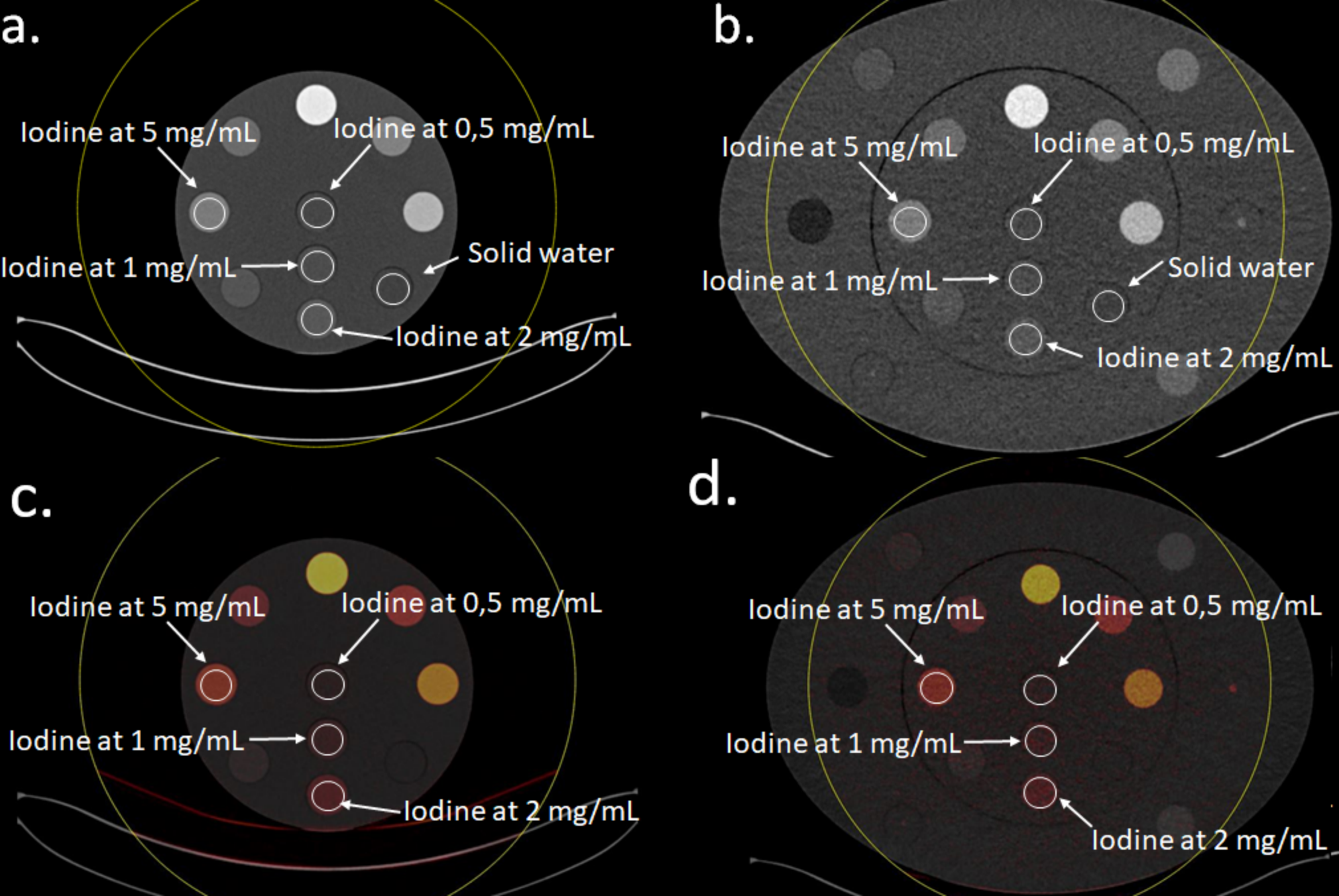
a.
Iodine at 5 mg/mL
Iodine at 0,5 mg/mL
Iodine at 1 mg/mL
Solid water
Iodine at 2 mg/mL
b.
Iodine at 5 mg/mL
Iodine at 0,5 mg/mL
Iodine at 1 mg/mL
Solid water
Iodine at 2 mg/mL
c.
Iodine at 5 mg/mL
Iodine at 0,5 mg/mL
Iodine at 1 mg/mL
Iodine at 2 mg/mL
d.
Iodine at 5 mg/mL
Iodine at 0,5 mg/mL
Iodine at 1 mg/mL
Iodine at 2 mg/mL

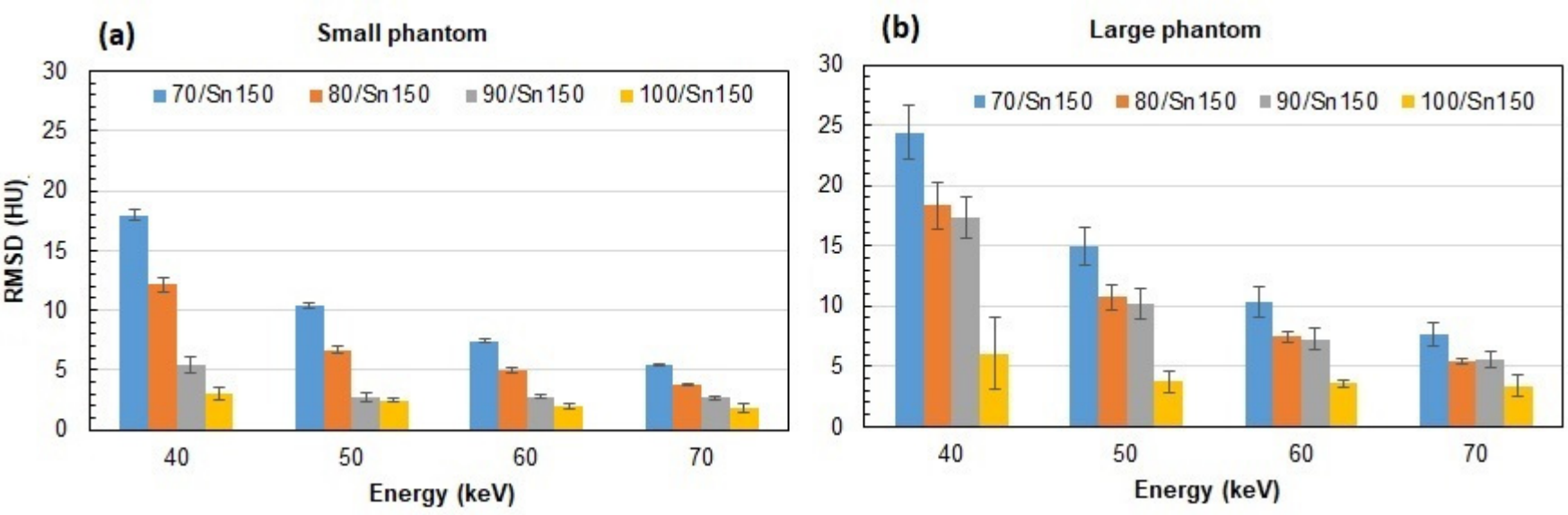
(a)
Small phantom
70/Sn150
80/Sn150
90/Sn150
100/Sn150
RMSD (HU)
30
25
20
15
10
5
0
40
50
60
70
Energy (keV)
(b)
Large phantom
70/Sn150
80/Sn150
90/Sn150
100/Sn150
30
25
20
15
10
5
0
40
50
60
70
Energy (keV)

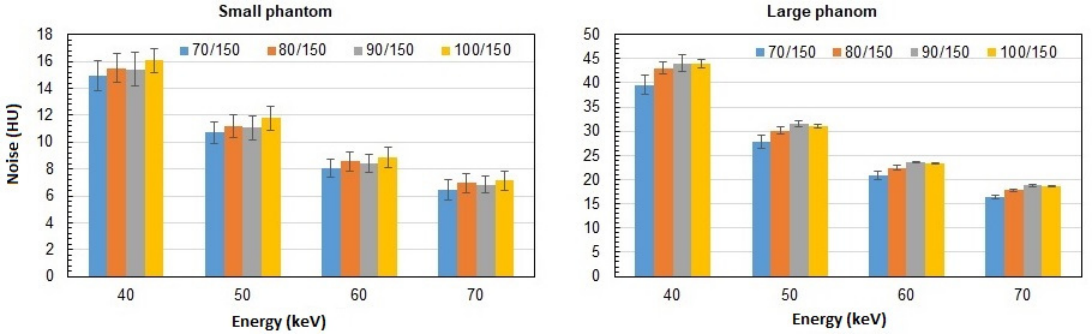
Small phantom
Noise (HU)
70/150
80/150
90/150
100/150
0
2
4
6
8
10
12
14
16
18
40
50
60
70
Energy (keV)
Large phanom
70/150
80/150
90/150
100/150
0
5
10
15
20
25
30
35
40
45
50
40
50
60
70
Energy (keV)

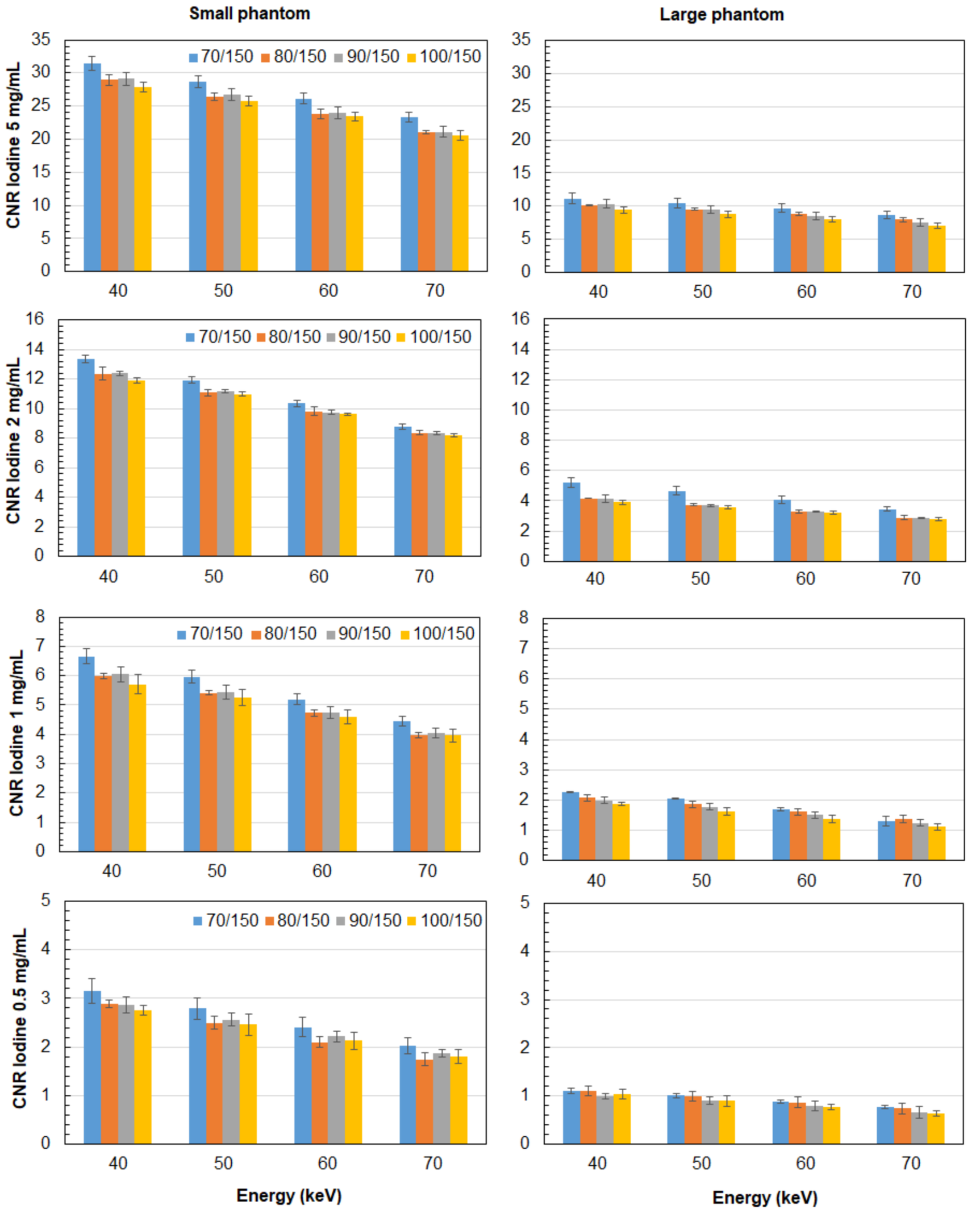
Small phantom
Large phantom
CNR Iodine 5 mg/mL
CNR Iodine 2 mg/mL
CNR Iodine 1 mg/mL
CNR Iodine 0.5 mg/mL
70/150
80/150
90/150
100/150
40
50
60
70
Energy (keV)